

## ON A MODEL OF COAL COMBUSTION

JINDŘICH MAKOVIČKA<sup>1</sup>, VLADIMÍR HAVLENA<sup>2</sup>, MICHAL BENEŠ<sup>1</sup>

**Abstract.** We describe behavior of the air-coal mixture using two sets of Navier-Stokes equations for gas and particle phases. The undergoing chemical reactions are described by Arrhenian kinetics (reaction rate proportional to  $\exp\left(-\frac{E}{RT}\right)$ , where T is temperature). We also consider the aerodynamic forces between the gas and particle phases, and the heat transfer via conduction and radiation. The system of PDEs is discretized using the Finite Volume Method and an Advection Upstream Splitting Method as the Riemann solver. The resulting ODEs are solved using the 4th order Runge-Kutta method. Results regarding numerical convergence estimation and parallelization efficiency are presented.

**AMS subject classifications.** 35L65, 76M12, 80A20

**Key words.** Navier-Stokes equations, heat transfer, reactive flow, finite-volume method

**1. Introduction.** The main motivation of the combustion model research is its future inclusion in the current model of the steam generator [4], to use this model for development of control systems for the industrial installation. Another purpose for the combustion model is the optimization of the production of the nitrogen oxides, which strongly depends on the temperature distribution, and thus can be controlled by intelligent distribution of fuel and oxygen into the burners. Because the experiments on a real device are prohibitively cumbersome and expensive, in extreme cases even hazardous, the only way to test the behavior of the furnace is mathematical modelling.

An industrial pulverized coal furnace (for schematics, see Figure 1.1) is basically a vertical channel with square cross-section. The dimensions are determined by the power generation requirements from the order of meters to tens of meters. In the case we model, the furnace has 30 meters in height and 7 meters in width, 49 m<sup>2</sup> cross-section. Power production of such a furnace is about 90 MW, and the furnace coupled with a steam generator is capable of producing about 100 tons of pressurized superheated steam per hour.

In the bottom of the channel walls, there are several burners — jets where the mixture of the air and coal pulver is injected. The mixture then flows up and burns, while it transfers some of the combustion heat to the walls containing the water pipes.

At the top, the heated flue gas continues to flow to the superheater channel where further heat exchange occurs, and this has already been covered by [4]. Our main concern is now modelling of the processes in the area, where the coal gets burnt.

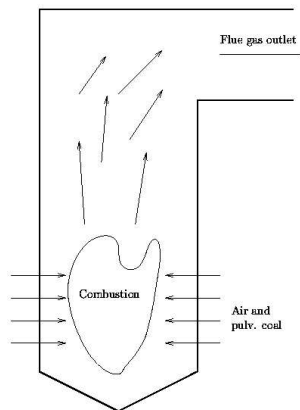


**Fig. 1.1:** Schematics of a coal furnace

<sup>1</sup>Faculty of Nuclear Sciences and Physical Engineering Czech Technical University in Prague, Czech Republic, Trojanova 13, 120 00 Praha 2

<sup>2</sup>Faculty of Electrical Engineering, Czech Technical University in Prague, Czech Republic, Karlovo nám. 13, 121 35 Praha 2

**2. Mathematical model.** In our simulation of a furnace with burners on two sides, we currently consider a 2D approximation of an original 3D problem. The mathematical model of combustion is based on two sets of Navier-Stokes equations, one for the gas component, one for the coal particle component. Both components are further divided into two phases — the gas component is treated as a mixture of oxygen and the rest of the gases, which do not participate in the combustion processes. Similarly, the coal component is divided into the combustible part (around 70%) and the incombustible part.

The respective species are denoted by the following indices:

- gas — denotes all variables belonging to the total amount of gas
- O2 — all variables belonging to the oxygen gas phase
- coal — all variables belonging to the total amount of coal
- coal\_comb — all variables belonging to the combustible part of coal
- coal\_ash — all variables belonging to the incombustible part of coal

The right-hand sides of the equations contain additional terms for external forces, heat transfer by conduction and radiation, and chemical kinetics.

The gas phase is described by the following equations: equation of balance for total mass of the gas component

$$\frac{\partial \rho_{\text{gas}}}{\partial t} + \frac{\partial(\rho_{\text{gas}} u_{\text{gas}})}{\partial x} + \frac{\partial(\rho_{\text{gas}} v_{\text{gas}})}{\partial y} = -n_{\text{coal}} \frac{dm_{\text{coal}}}{dt}, \quad (2.1)$$

where  $\rho_{\text{gas}}$  is the flue gas mass density, and  $u_{\text{gas}}, v_{\text{gas}}$  are the gas velocity components. The right-hand side term describes the flue gas production due to the evaporation of the coal during combustion. The term  $n_{\text{coal}}$  is the coal particle numeric density, i.e. number of particles per unit volume,  $\frac{dm_{\text{coal}}}{dt}$  the particle mass change rate.

The above equation of mass balance is accompanied by the equation of mass balance for the oxygen:

$$\frac{\partial \rho_{\text{O2}}}{\partial t} + \frac{\partial(\rho_{\text{O2}} u_{\text{gas}})}{\partial x} + \frac{\partial(\rho_{\text{O2}} v_{\text{gas}})}{\partial y} = -X_{\text{O2}} n_{\text{coal}} \frac{dm_{\text{coal}}}{dt}, \quad (2.2)$$

where  $X_{\text{O2}}$  is the mass stoichiometric ratio (amount of oxygen per 1 kg of fuel) for the combustion reaction.

Equations of momentum conservation

$$\begin{aligned} & \frac{\partial(\rho_{\text{gas}} u_{\text{gas}})}{\partial t} + \frac{\partial}{\partial x}(p + \rho_{\text{gas}} u_{\text{gas}}^2) + \frac{\partial(\rho_{\text{gas}} u_{\text{gas}} v_{\text{gas}})}{\partial y} = \\ & = \mu_{\text{gas}}(u_{\text{gas}_{xx}} + u_{\text{gas}_{yy}}) + \frac{\mu_{\text{gas}}}{3}(u_{\text{gas}_{xx}} + v_{\text{gas}_{xy}}) - \\ & - \beta(u_{\text{gas}} - u_{\text{coal}}) - u_{\text{coal}} n_{\text{coal}} \frac{dm_{\text{coal}}}{dt}, \end{aligned} \quad (2.3)$$

and

$$\begin{aligned} & \frac{\partial(\rho_{\text{gas}} v_{\text{gas}})}{\partial t} + \frac{\partial}{\partial y}(p + \rho_{\text{gas}} v_{\text{gas}}^2) + \frac{\partial(\rho_{\text{gas}} u_{\text{gas}} v_{\text{gas}})}{\partial x} = \\ & = \mu_{\text{gas}}(v_{\text{gas}_{xx}} + v_{\text{gas}_{yy}}) + \frac{\mu_{\text{gas}}}{3}(u_{\text{gas}_{yx}} + v_{\text{gas}_{yy}}) - \\ & - \rho_{\text{gas}} g - \beta(v_{\text{gas}} - v_{\text{coal}}) - v_{\text{coal}} n_{\text{coal}} \frac{dm_{\text{coal}}}{dt}, \end{aligned} \quad (2.4)$$

where

$$\beta = \frac{3}{4} C_D d_{\text{coal}}^2 \rho_{\text{gas}} |\vec{v}_{\text{gas}} - \vec{v}_{\text{coal}}|, \quad (2.5)$$

$C_D$  is the empirically calculated aerodynamic friction coefficient, dependent on the Reynolds number (see [2])

$$C_D = \begin{cases} \frac{24}{\text{Re}} \left(1 + \frac{\text{Re}^{0.6667}}{6}\right) & \text{Re} < 1000 \\ 0.44 & \text{Re} \geq 1000. \end{cases} \quad (2.6)$$

The Reynolds number for the particles is defined as

$$\text{Re} = |\vec{v}_{\text{gas}} - \vec{v}_{\text{coal}}| d_{\text{coal}} / \nu_{\text{gas}}, \quad (2.7)$$

where  $\nu_{\text{gas}} = \mu_{\text{gas}} / \rho_{\text{gas}}$  is the kinematic viscosity of gas related to the viscosity of gas. The particle diameter is calculated as

$$d_{\text{coal}} = 2 * \left( \frac{3}{4\pi} \frac{\rho_{\text{coal}}}{\rho_{0\text{coal}} n_{\text{coal}}} \right)^{-3}, \quad (2.8)$$

where  $\rho_{0\text{coal}}$  is the raw density of coal, as opposed to  $\rho_{\text{coal}}$ , which is the amount of coal in  $1\text{ m}^2$  of flue gas. The last equation describes the conservation of energy (with  $h$  denoting specific enthalpy of either coal or gas)

$$\begin{aligned} \frac{\partial(\rho_{\text{gas}} h_{\text{gas}})}{\partial t} + \frac{\partial(\rho u_{\text{gas}} h_{\text{gas}})}{\partial x} + \frac{\partial(\rho v_{\text{gas}} h_{\text{gas}})}{\partial y} = \\ = -n_{\text{coal}} \frac{dm_{\text{coal}}}{dt} h_{\text{comb}} - n_{\text{coal}} \frac{dm_{\text{coal}}}{dt} h_{\text{coal}} + q_r + q_c + q_s, \end{aligned} \quad (2.9)$$

where the right-hand side terms are the heat of combustion, enthalpy increase due to phase change, heat transfer by radiation, heat transfer by conduction, and heat source/sink. The heat transfer terms are computed as follows:

$$q_c = \lambda(T_{\text{gas}xx} + T_{\text{gas}yy}), \quad (2.10)$$

for the transfer by conduction, with  $\lambda$  being the heat transfer coefficient, and

$$q_r = \frac{1}{|\Omega|} K \int_{\Omega} \sigma T_{\text{gas}}^4 dV, \quad (2.11)$$

where  $\sigma$  is Steffan-Boltzmann constant, for the transfer by radiation. Constant  $K$  determines the absorbtion and emission properties of the gas. To simplify the computation, the radiation energy is assumed to be distributed uniformly throughout all the computational region. The heat sink term is nonzero only in the edge computation cells and describes the energy exchange with the walls of the furnace via conduction and radiation:

$$q_s = A(T_{\text{gas}} - T_{\text{wall}}) + B(T_{\text{gas}}^4 - T_{\text{wall}}^4). \quad (2.12)$$

$A$  and  $B$  are constants depending on furnace wall width and heat transfer coefficient between the computational region and the surroundings.

The particle mass change rate is currently described by one-step Arrhenian kinetics

$$\frac{dm_p}{dt} = -A_v m_p^\alpha [O_2]^\gamma \exp\left(-\frac{E_v}{RT_p}\right), \quad (2.13)$$

where  $m_p$  is the particle combustible mass,  $R$  the molar gas constant,  $M$  molar mass,  $A_v, \gamma, E_v$  are empirical constants,  $[O_2]$  oxygen concentration and  $T_p$  is the particle temperature.

These equations are accompanied by the equation of state, as usually:

$$p = (\kappa - 1)\rho_{\text{gas}} \left( e_{\text{gas}} - \frac{1}{2}v_{\text{gas}}^2 \right). \quad (2.14)$$

Here,  $\kappa = \frac{c_p}{c_v}$  is the Poisson constant and  $e_{\text{gas}}$  is the gas energy per unit mass.

The coal particle phase is modelled by the same set of equations, with two main differences. First, the pressure terms do not appear in the equations, as the pressure forces among the scattered particles are negligible, and the particles are only passively transported by their advection velocity. Second, there is one more equation for the numeric particle density (number of particles per unit volume), similar to the equation of mass balance:

$$\frac{\partial n_{\text{coal}}}{\partial t} + \frac{\partial(n_{\text{coal}}u_{\text{coal}})}{\partial x} + \frac{\partial(n_{\text{coal}}v_{\text{coal}})}{\partial y} = 0. \quad (2.15)$$

The next one is the equation of mass balance for the coal

$$\frac{\partial \rho_{\text{coal}}}{\partial t} + \frac{\partial(\rho_{\text{coal}}u_{\text{coal}})}{\partial x} + \frac{\partial(\rho_{\text{coal}}v_{\text{coal}})}{\partial y} = n_{\text{coal}} \frac{dm_{\text{coal}}}{dt}, \quad (2.16)$$

and for the incombustible part

$$\frac{\partial \rho_{\text{coal\_ash}}}{\partial t} + \frac{\partial(\rho_{\text{coal\_ash}}u_{\text{coal}})}{\partial x} + \frac{\partial(\rho_{\text{coal\_ash}}v_{\text{coal}})}{\partial y} = 0. \quad (2.17)$$

Equations of momentum of coal are

$$\begin{aligned} & \frac{\partial(\rho_{\text{coal}}u_{\text{coal}})}{\partial t} + \frac{\partial}{\partial x}(\rho_{\text{coal}}u_{\text{coal}}^2) + \frac{\partial(\rho_{\text{coal}}u_{\text{coal}}v_{\text{coal}})}{\partial y} = \\ & = \mu_{\text{coal}}(u_{\text{coal}xx} + u_{\text{coal}yy}) + \frac{\mu_{\text{coal}}}{3}(u_{\text{coal}xx} + v_{\text{coal}xy}) + \\ & + \beta(u_{\text{gas}} - u_{\text{coal}}) + u_{\text{coal}}n_{\text{coal}} \frac{dm_{\text{coal}}}{dt}, \end{aligned} \quad (2.18)$$

and

$$\begin{aligned} & \frac{\partial(\rho_{\text{coal}}v_{\text{coal}})}{\partial t} + \frac{\partial}{\partial y}(\rho_{\text{coal}}v_{\text{coal}}^2) + \frac{\partial(\rho_{\text{coal}}u_{\text{coal}}v_{\text{coal}})}{\partial x} = \\ & = \mu_{\text{coal}}(v_{\text{coal}xx} + v_{\text{coal}yy}) + \frac{\mu_{\text{coal}}}{3}(u_{\text{coal}yx} + v_{\text{coal}yy}) - \\ & - \rho_{\text{coal}}g + \beta(v_{\text{gas}} - v_{\text{coal}}) + v_{\text{coal}}n_{\text{coal}} \frac{dm_{\text{coal}}}{dt}, \end{aligned} \quad (2.19)$$

where  $\mu_{\text{coal}}$  is the coal-pulver viscosity. The equation of energy for the coal is not used, as the energy exchange between coal and other phases is omitted and for coal, the energy is also just passively transported by the advection velocity, like the mass, so it does not have any influence on the above equations of the coal flow.

**3. Numerical algorithm.** For numerical solution of the equations, Finite Volume Method is used. For left hand sides, Advection Upstream Splitting Method (see [3]) is used to approximate fluxes in the FVM formulation, while edge dual-volume approximation is used to approximate the second order derivatives on the right-hand sides.

**AUSM Riemann solver.** Here we briefly summarize the algorithm of the AUSM Riemann solver. Note that the following equations are already in the form after transformation into normal/tangential coordinates of a particular edge between two finite volumes. See e.g. [6] for more details on application of Riemann solvers. The terms corresponding to the supersonic velocities are not used in our application, as the velocities are much lower, but they are used in the method description for the sake of completeness. The basic idea of the method is to split the Euler equations into convection terms (containing the velocity  $v$  and pressure terms  $p$ ). Then, for the convection terms, van Leer splitting is used to compute the numerical flux over the cell boundary, while for pressure terms another splitting is used, more suitable to the fact that the pressure terms are governed by the acoustic wave speeds.

Thus, for the pressure terms, we obtain

$$\mathbf{F}_{1/2}^c = u_{1/2} \begin{pmatrix} \rho \\ \rho u \\ \rho v \\ (\rho e + p) \end{pmatrix}_{L/R} = M_{1/2} \begin{pmatrix} \rho a \\ \rho a u \\ \rho a v \\ (a(\rho e + p)) \end{pmatrix}_{L/R}, \quad (3.1)$$

where

$$(\cdot)_{L/R} \begin{cases} (\cdot)_L, & \text{if } M_{1/2} \geq 0 \\ (\cdot)_R, & \text{otherwise.} \end{cases} \quad (3.2)$$

The cell interface Mach number is then the sum of Mach numbers from left and right

$$M_{1/2} = M_L^+ + M_R^-, \quad (3.3)$$

where

$$M^\pm = \begin{cases} \pm \frac{1}{4}(M \pm 1)^2 & |M| \leq 1; \\ \frac{1}{2}(M \pm |M|) & \text{otherwise.} \end{cases} \quad (3.4)$$

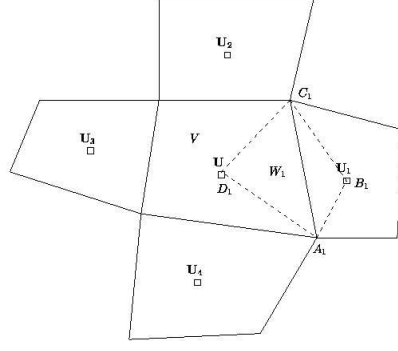
The pressure terms are split as follows:

$$p_{1/2} = p_L^+ + p_R^-, \quad (3.5)$$

$$p^\pm = \begin{cases} \frac{p}{4}(M \pm 1)^2(2 \mp M) & |M| \leq 1; \\ \frac{p}{2}(M \pm |M|)/M & \text{otherwise.} \end{cases} \quad (3.6)$$

The whole scheme can be finally written as the formula for the variable values at the cell interface:

$$\begin{pmatrix} \rho u \\ \rho u^2 + p \\ \rho u v \\ (\rho + E)u \end{pmatrix} = M_{1/2} \frac{1}{2} \left[ \begin{pmatrix} \rho a \\ \rho a u \\ \rho a v \\ \rho(p + E)a \end{pmatrix}_L + \begin{pmatrix} \rho a \\ \rho a u \\ \rho a v \\ \rho(p + E)a \end{pmatrix}_R \right] - \frac{1}{2} |M_{1/2}| \Delta_{1/2} \begin{pmatrix} \rho a \\ \rho a u \\ \rho a v \\ \rho(p + E)a \end{pmatrix} + \begin{pmatrix} 0 \\ p_L^+ + p_R^- \\ 0 \\ 0 \end{pmatrix}, \quad (3.7)$$

FIG. 3.1. Dual volume  $W_1$  for 1st edge of the volume  $V$ 

where  $\Delta_{1/2}\{\cdot\} = \{\cdot\}_R - \{\cdot\}_L$ .

**Second-order derivatives.** To compute the second order derivatives of the state variables at the right-hand sides, we use the dual volume approximation — the derivatives are transformed to a cell average by applying the Green theorem twice:

$$\int_V (f_x + g_y) dx dy = \oint_{\partial V} f dy - g dx. \quad (3.8)$$

Our goal is to obtain an approximation of average value of the Laplacian  $u_{xx} + u_{yy}$  on the volume  $V$ . By first application of the Green theorem on the integral and approximation of the boundary values with constants, we obtain

$$\frac{1}{|V|} \int_V (u_{xx} + u_{yy}) dx dy = \frac{1}{|V|} \oint_{\partial V} u_x dy - u_y dx = \frac{1}{|V|} \sum_{i=1}^N u_x|_i \Delta y_i - u_y|_i \Delta x_i, \quad (3.9)$$

where  $\Delta y_i$  and  $\Delta x_i$  are  $x$  and  $y$  coordinate differences for respective edge of the volume  $V$ . To calculate the sum, we need values of  $u_x$  and  $u_y$  on the boundaries. They are obtained by a subsequent application of the Green theorem on the dual volume  $W_i$  (Fig. 3.1,  $W_1$  is marked by dashed line):

$$\int_{W_i} (f_x + g_y) dx dy = \oint_{\partial W_i} f dy - g dx. \quad (3.10)$$

To calculate  $u_x|_1$ , by stating  $f = u$ ,  $g = 0$  we obtain

$$\int_{W_i} u_x dx dy = \oint_{\partial W_i} u dy = \sum_{j=1}^4 \mathbf{U}'_j \Delta y_j, \quad (3.11)$$

where  $\Delta y_j$  is  $y$  coordinate difference for respective edge of the dual volume  $W_1$ . Thus,  $u_x|_1$  can be approximated by

$$u_x|_1 \approx \frac{1}{|W_1|} \sum_{j=1}^4 \mathbf{U}'_j \Delta y_j. \quad (3.12)$$

The values at the vertices of  $V$  are interpolated as averages of the values in their neighboring cells, weighted by cell areas. Values of  $\mathbf{U}'_1, \mathbf{U}'_2, \mathbf{U}'_3, \mathbf{U}'_4$  are approximated

using the values on cells and at vertices as follows.

$$\mathbf{U}'_1 = \frac{1}{2}(\mathbf{U}_{A_1} + \mathbf{U}_{B_1}), \quad \mathbf{U}'_2 = \frac{1}{2}(\mathbf{U}_{B_1} + \mathbf{U}_{C_1}), \quad (3.13)$$

$$\mathbf{U}'_3 = \frac{1}{2}(\mathbf{U}_{C_1} + \mathbf{U}_{D_1}), \quad \mathbf{U}'_4 = \frac{1}{2}(\mathbf{U}_{D_1} + \mathbf{U}_{A_1}). \quad (3.14)$$

Calculation of  $u_y|_1$  is similar. The same approach is also used for the mixed derivatives appearing in the viscosity terms in the Navier-Stokes equations.

**4. Implementation.** The simulation is developed as a stand-alone program in C. FVM Advection Upstream Splitting scheme, as mentioned before, is used to approximate the PDEs by a set of ODEs in time, and 4-th order standard Runge-Kutta method is used to compute the solution of the ODE system. The equations for both phases are discretized using the same method and are solved by one numerical solver simultaneously.

During one time step, the time step size is determined first by finding the maximum PDE eigenvalue for the gas phase over the region, and applying the CFL condition.

**5. Parallelization and benchmarking.** For parallelization, the MPI framework (<http://www.mpi-forum.org/docs/>) has been used.

To make the above code work in parallel, each node needs to receive the data from neighboring cells of its “own” cell after each computation step. Secondly, computation of the length of the time step has to be done cooperatively using `MPI_Reduce` and `MPI_Broadcast` functions to determine the global maximum of the PDE eigenvalues.

As there are no explicit requirements on the mesh subdivision, the initialization routine has to locate all the neighbors and resolve the demands on the cells.

This leads to more complicated initialization of the code, but the further communication is already simple and the code allows very general subdivisions of the grid. To test an arbitrary subdivision, even a uniform random distribution of the cells among the nodes has been considered, and the simulation still produced identical results, although with extremely low performance, because of the communication overhead. For practical computations, MPI functions for node distribution on cartesian coordinates (`MPI_Cart_rank`) were used. For a grid of 40x400 cells, the simulation benchmark results are summarized in Figure 5.1 and Table 5.1, which represent dependency of the number of computed time steps per second (“Performance” column) on the number of CPUs used. Computational efficiency of a parallel algorithm is defined as follows (also see [5]):

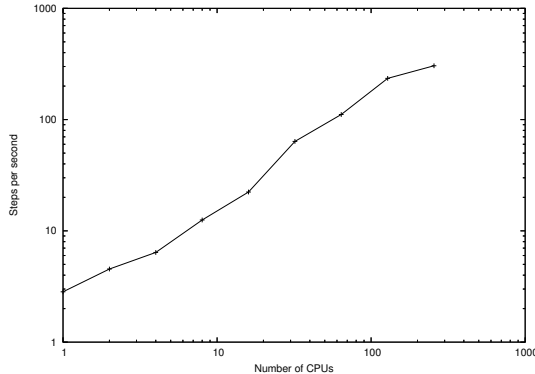


**Fig. 5.1:** Parallel scalability

on cartesian coordinates (`MPI_Cart_rank`) were used. For a grid of 40x400 cells, the simulation benchmark results are summarized in Figure 5.1 and Table 5.1, which represent dependency of the number of computed time steps per second (“Performance” column) on the number of CPUs used. Computational efficiency of a parallel algorithm is defined as follows (also see [5]):

$$\text{Speedup} = \frac{\text{Runtime on 1 CPU}}{\text{Runtime on } N \text{ CPUs}}, \quad \text{Efficiency} = \frac{\text{Speedup}}{\text{Number of CPUs}}.$$

We have chosen a structured grid, to be able to debug the code by comparison with a finite difference method. However, the FVM code allows to use an arbitrary grid.

To estimate convergence of the method, a number of testing runs on meshes with different size were performed. We used meshes with resolutions from 10x100 to 40x400, and compared the results with a 80x800 mesh. The results were compared in  $L_1$  and  $L_2$  norms in space, and either  $L_1$  or  $L_2$  or  $L_\infty$  in time. Tables 5.2 and 5.3 contain the results with EOC for each type of error indicated [1]. EOC between two scales is defined as

$$\text{EOC} = \frac{\ln(E_2/E_1)}{\ln(h_2/h_1)},$$

where  $E_2$  and  $E_1$  are numerical errors, and  $h_2$  and  $h_1$  are the grid sizes.

TABLE 5.1  
*Efficiency of the parallel computation.*

CPUs	Performance	Speedup	Eff
1	2.830687	1.000	1.000
2	4.539230	1.604	0.802
4	6.394759	2.259	0.565
8	12.526646	4.425	0.553
16	22.344537	7.894	0.493
32	63.654814	22.487	0.703
64	111.208353	39.287	0.614
128	234.860252	82.969	0.648
256	304.744175	107.657	0.421

TABLE 5.2  
*Convergence of the temperature profile. Grid resolution is  $(N * 5 \times N * 50)$*

$N$	$L_{1,1}$	EOC	$L_{2,2}$	EOC	$L_{1,\infty}$	EOC	$L_{2,\infty}$	EOC
2	28702	—	2266	—	4795	—	995	—
3	21416	0.722	1907	0.426	3671	0.659	800	0.538
4	17663	0.670	1634	0.536	3020	0.678	688	0.523
5	16241	0.376	1559	0.210	2689	0.521	663	0.164
6	14371	0.671	1456	0.377	2423	0.571	630	0.284
7	12387	0.964	1356	0.460	2133	0.826	585	0.474
8	11425	0.606	1327	0.161	2016	0.422	573	0.163

TABLE 5.3  
*Convergence of the velocity profile. Grid resolution is  $(N * 5 \times N * 50)$*

$N$	$L_{1,1}$	EOC	$L_{2,2}$	EOC	$L_{1,\infty}$	EOC	$L_{2,\infty}$	EOC
2	2849	1.000	178	1.000	934	1.000	119	1.000
3	2287	0.541	144	0.529	849	0.235	106	0.289
4	1900	0.645	118	0.677	609	1.156	79	1.035
5	1762	0.336	112	0.250	490	0.971	70	0.510
6	1538	0.747	100	0.639	383	1.360	60	0.892
7	1338	0.903	85	1.060	323	1.108	49	1.229
8	1182	0.927	77	0.737	265	1.483	44	0.827



TABLE 5.4  
Simulation parameters

Parameter	Symbol	Value	Unit
grav. acceleration	$g$	9.81	$\text{m s}^{-2}$
gas heat capacity	$c_V$	1037.0	$\text{J kg}^{-1} \text{K}^{-1}$
molar mass of gas	$M$	0.02801	$\text{kg mol}^{-1}$
raw coal density	$\rho$	1345.0	$\text{kg m}^{-3}$
coal particle radius	$r_{\text{coal}}$	$0.2 \cdot 10^{-3}$	m
coal heat capacity	$c_V$	1000	$\text{J kg}^{-1} \text{K}^{-1}$
furnace cross-section	$S$	49.0	$\text{m}^2$
mass throughput of the gas	$q$	48.0	$\text{kg m}^{-2} \text{s}^{-1}$
initial pressure	$p_{\text{ini}}$	$1.0 \cdot 10^5$	Pa
initial temperature	$T_{\text{ini}}$	630	$^{\circ}\text{C}$
O <sub>2</sub> concentration at the inlet	$[O_2]_{\text{in}}$	21	%
gas temperature at the inlet	$T_{\text{in}}$	230	$^{\circ}\text{C}$
pressure at the inlet	$p_{\text{in}}$	$1.0 \cdot 10^5$	Pa
kg coal per 1kg gas at inlet		0.16	kg
incombustible coal matter at inlet		30	%
heat of combustion of the combustible part		24558	$\text{kJ kg}^{-1}$
heat conductivity of the gas		24.0	$\text{W m}^{-1} \text{K}^{-1}$
gas – wall heat transfer coef (conduction)		30.0	$\text{W m}^{-2} \text{K}^{-1} \text{s}^{-1}$
gas – wall heat transfer coef (radiation)		$0.6 \cdot 10^{-8}$	$\text{W m}^{-2} \text{K}^{-4} \text{s}^{-1}$
temperature of the wall		300	$^{\circ}\text{C}$
width of the side wall		7.0	m
amount of oxygen per 1 kg burnt coal		1.65	kg

Outputs in Figures 5.2, 5.3, 5.4 were obtained by a simulation on a grid of 40x400 cells of a symmetrical channel 30x7m in size, with 2x4 burners (situated in the left part of the top and bottom edges). Flue gas flow rate was 48 kg/s, which corresponds with 125 t/h steam production mode. Complete list of the physical parameters used in the computation is summarized in Table 5.4.

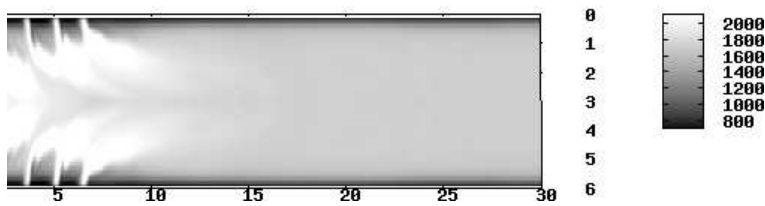


FIG. 5.2. Temperature profile in degrees K

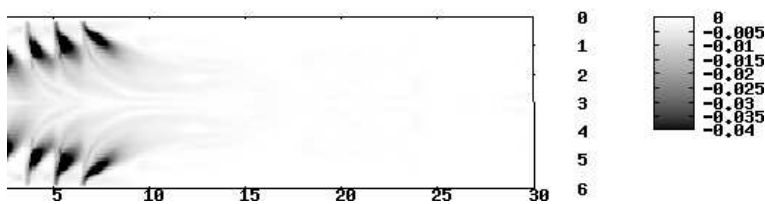


FIG. 5.3. Combustion rate (amount of burnt fuel per second) in  $\text{kg s}^{-1} \text{m}^{-3}$

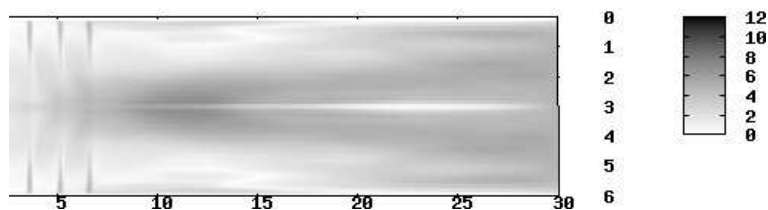


FIG. 5.4. *Velocity absolute magnitude in  $m s^{-1}$*

**6. Conclusion.** We have developed a simple mathematical model, which approximates the combustion process in an industrial furnace. As an outlook to the future, mainly the following improvement possibilities are being considered:

- Implementation of a more precise model of the coal combustion.
- Implementation of a turbulence model.
- More detailed model of the radiation, using an integral-differential equation of the radiation.

**7. Acknowledgements.** First and second author acknowledge partial support of the Czech Ministry of Industry and Trade through the grant No. 1H-PK/22 “Advanced control and optimization for power generation” and third author acknowledges partial support of the Czech Ministry of Education, Youth and Sport through the research plan No. MSM:6840770010 “Applications of Mathematics in Technology and Physics”. Part of the work has been performed under the Project HPC-EUROPA (RII3-CT-2003-506079), with the support of the European Community — Research Infrastructure Action under the FP6 “Structuring the European Research Area” Programme.

#### REFERENCES

- [1] G. DZIUK, *Discrete anisotropic curve shortening flow*, Siam Journal of Numerical Analysis, 36 (1999), pp. 1808–1830
- [2] Y.C. GUO, C.K. CHAN, *A Multi-fluid model for simulating turbulent gas-particle flow and pulverized coal combustion*, FUEL 79 (2000) 1467–1476.
- [3] MENG-SING LIOU, C. STEFFEN, JR., *A New Flux Splitting Scheme*, J. Comp. Phys., 1993, vol. 107, pp 23–29.
- [4] J. MAKVIČKA, V. HAVLENA AND M. BENEŠ, *Mathematical modelling of steam and flue gas flow in a heat exchanger of a steam boiler*, ALGORITMY 2002, peer reviewed Proceedings of contributed papers and posters, pp. 171–178, Publ. house of STU, 2002, ISBN 80-227-1750-9
- [5] J. MIKYŠKA, M. ŠENKÝŘ AND M. BENEŠ, *Application of parallel computing techniques for problems of degenerate diffusion*, in *Numerical Mathematics and Advanced Applications*, ENUMATH 2003 (peer reviewed proceedings), pp. 756–766, eds. M. Feistauer, V. Dolejší, P. Knobloch, K. Najzar, Springer Verlag, 2004, ISBN 3-540-21460-7
- [6] E. F. TORO, *Riemann Solvers and Numerical Methods for Fluid Dynamics*, Springer Verlag, Berlin, 1997